Fast ignition transport simulations for NIF

2010 J. Phys.: Conf. Ser. 244 022065

(http://iopscience.iop.org/1742-6596/244/2/022065)

Journal of Physics: Conference Series **244** (2010) 022065 doi:10.1088/1742-6596/244/2/022065

Fast ignition transport simulations for NIF

D. J. Strozzi, D. P. Grote, M. Tabak, B. I. Cohen, R. P. J. Town, A. J. Kemp

Lawrence Livermore National Laboratory, 7000 East Avenue, Livermore, CA 94550, USA

E-mail: strozzi2@llnl.gov

Abstract. This paper shows work at Lawrence Livermore National Lab (LLNL) devoted to modeling the propagation of, and heating by, a relativistic electron beam in a idealized dense fuel assembly for fast ignition [1]. The implicit particle-in-cell (PIC) code LSP is used. Experiments planned on the National Ignition Facility (NIF) in the next few years using the Advanced Radiography Capability (ARC) short-pulse laser motivate this work. We demonstrate significant improvement in the heating of dense fuel due to magnetic forces, increased beam collimation, and insertion of a finite-radius carbon region between the beam excitation and fuel regions.

1. Simulation approach

A basic dilemma in fast ignition (FI) transport simulation is capturing the physics of the relativistic electron beam, while affordably describing the dense, cold ($\lesssim 1$ keV) background plasma. Resolving high-frequency Langmuir waves is prohibitive, and not essential since they are strongly damped by high collisionality. Light waves also need not be resolved, since the plasma is far above critical density for laser light. To solve this problem we use the implicit particle-in-cell (PIC) method, which numerically damps unresolved modes ($\omega\Delta t \gg 1$) while fully resolving the physics for $\omega\Delta t \lesssim 1$ subject to some numerical modification of the dielectric shielding [2]. Unlike some hybrid approaches which use simplified Maxwell equations or a resistive Ohm's law, this method can simulate the complete physics at low density and *smoothly* transition to an effectively reduced description at high density.

We use the PIC code LSP [3] in 2D cylindrical r-z geometry for our simulations. We employ an electromagnetic direct-implicit (as opposed to implicit-moment) PIC algorithm related to that of Ref. [4]. However, the "implicit magnetization" term is neglected. In the numerical field equations (see Eq. (97a) in [2]), the term containing the implicit magnetization is smaller than the term containing the electrostatic "implicit susceptibility" (included in LSP) by roughly the factor $v_e\Delta t/2L$, where v_e is the electron drift speed and L is a length scale. For the extreme case of $v_e = c$ and $L = \Delta x$, this term is $< 1/2$ as long as the light Courant condition is respected (which we always do). We run with the fully-damped D1 scheme [5]. We do not simulate the short-pulse LPI, but instead excite an electron beam with a specified distribution from the background plasma. The E and B fields are found with an iterative ADI solver.

To reduce the cost of simulating the background plasma, we utilize LSP "fluid particles." They each carry mass, position, momentum (representing the drift of a thermal Maxwellian), and a temperature governed by an energy equation. Their evolution equations contain terms for fluid effects like heat conduction and pressure-gradient forces. These are automatically included in standard PIC with collisions, but must be explicitly added for fluid particles, whose momenta

do not reflect any thermal spread. The fluid-fluid collision rate is the classical one for a hot plasma, without taking Fermi degeneracy or electron-electron collisions into account; this gives a resistivity scaling like $T_e^{-3/2}$ where T_e is electron temperature. This may be inadequate for our conditions, and is being improved. We initially have nine fluid particles per cell per species, much less than would be needed by conventional PIC to resolve a thermal Maxwellian.

We extensively modified the collisions of the beam electrons off other species. We found LSP's original algorithm generated significant energy error. Our method scatters a test species off a field species, but not itself. This suffices for beam number densities much less than the background, which applies here. We follow a spatially grid-based method similar to Manheimer [6] and Lemons [7] (we adopt Lemons' spherical-coordinate algebra). We find cell-averaged field-species moments (e.g., density and drift velocity), and increment each test particle's momentum $\vec{u} = \gamma\vec{\beta}$. On average, this yields a deterministic energy loss, and stochastic heating and angular spread. In the field species' drift frame, $\vec{u}$ changes from $\vec{u}_0$ to $\vec{u}_0 + \Delta\vec{u}$ with

$$\Delta u = -\nu_{ud,j}\Delta t + [\nu_{us,j}\Delta t]^{1/2} N_u \quad (1)$$

$$\Delta\theta = [\nu_{\theta,j}\Delta t]^{1/2} N_\theta, \qquad \Delta\phi = 2\pi U_\phi \quad (2)$$

$u = |\vec{u}|$, (θ, ϕ) are the (polar, azimuthal) angles with respect to $\vec{u}_0$, U_ϕ is a uniform deviate on $[0, 1)$, and N_u, N_θ are normal deviates with zero mean and unit variance. $j = (e, i)$ for field (electron, ion) species. The inverse process, namely collisions of the field off test species, is done by energy and momentum conservation in each cell.

Our exact formulas are those of Davies [8], which essentially match Solodov's [9].

$$\nu_{ud,e} = \nu_{0,e}\beta^{-2}L_{ud}, \qquad \nu_{ud,i} = \nu_{us,j} = 0, \qquad \nu_{\theta,j} = 2\nu_{0,j}\gamma^{-2}\beta^{-3}L_{\theta,j} \quad (3)$$

$$L_{ud} = \ln\left[\frac{m_e c^2}{\hbar\omega_{pe}}\frac{\beta(\gamma-1)^{1/2}}{2^{1/2}}\right] + 9/16 + \gamma^{-1}(\ln 2 + 1/8)(-1 + 1/(2\gamma)) \quad (4)$$

$$L_{\theta,e} = \ln\Lambda - (1/2)(1 + \ln[2\gamma + 6]), \qquad L_{\theta,i} = \ln\Lambda - (1/2)(1 + \beta^2) \quad (5)$$

$\nu_{0,j} = 4\pi c r_e^2 n_j Z_j^2$, $r_e = e^2/(4\pi\epsilon_0 m_e c^2) \approx 2.82$ fm, $\Lambda = 2\lambda_{De} m_e c\gamma\beta/\hbar$, and λ_{De} is the background electron Debye length. The energy loss is appropriate for a fast electron scattering off a cold, dense background, such that all electrons are effectively free (Fermi's density effect dominates any ionization-energy effects [8]). Inclusion of nonzero field species temperature would give $\nu_{us,j} \neq 0$ (stochastic heating).

2. Calculations on an idealized NIF-ARC coupling target

We present LSP transport calculations for a compressed target appropriate to coupling (as opposed to ignition) experiments on NIF-ARC. ARC entails converting four NIF long-pulse beams (one quad) to a short-pulse laser. This should deliver $\approx$ 9 kJ of laser energy in a 5 ps pulse, at a wavelength of 1054 nm, into a spot with intensity half-width at half-max of ≈ 25 μm. We do not simulate the short-pulse laser, but instead excite an electron beam inside the simulation domain with a prescribed distribution function. In particular, we excite a beam with 4.8 kJ of kinetic energy (assuming a feasible laser to beam conversion efficiency of 53%) in a 5 ps flattop pulse, with linear ramps of 0.1 ps.

The beam distribution is $f/f_0 = n(\vec{r}, t) f_E(E) f_\theta(\theta)$ where $\int dE d\theta\, f = n$, n is the beam density, f_0 is a scale factor, and θ is the polar angle of $\vec{u}$ with respect to the u_z axis. $f_E(E) = \exp[-E/(0.3\,\mathrm{MeV})] + 0.05\exp[-E/(3\,\mathrm{MeV})]$ for kinetic energy E between 0.2 and 10 MeV, and $f_E = 0$ otherwise. We commonly see such two-temperature distributions in explicit-PIC simulations of the short-pulse LPI. In angle, we use $f_\theta(\theta) = \sin\theta\exp[-(\theta/\Delta\theta)^2]$; the $\sin\theta$ factor is absent if one considers number per *solid* angle. The density profile is

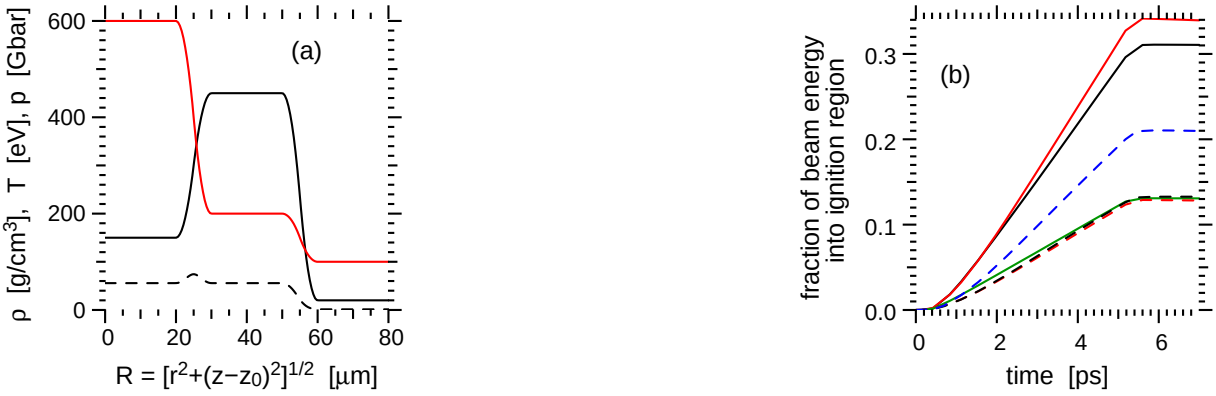

Figure 1. (a) Initial plasma conditions for base case. Solid black: mass density ρ, solid red: temperature (same for all species), dash black: total pressure (initial peak value: 74 Gbar). (b) Increase in thermal energy in ignition region, as a fraction of total added beam energy. Solid black: base case; solid red: base case but material is pure D instead of CD; solid green: base case without magnetic forces; dashed black: base case but $\Delta\theta = 60°$; dashed red: pure D with $\Delta\theta = 60°$; dashed blue: D with C wire, $\Delta\theta = 60°$.

$n = n_0(t)\exp[-(r/25\mu\text{m})^4]$, with $n_0(t)$ giving the temporal pulse. We do not vary f_E or f_θ in space or time. For this beam, the peak intensity and n_0 are $6.4\cdot10^{19}$ W/cm^2 and $1.0\cdot10^{22}$/cm^3, or about 10 times the critical density for ARC. The beam electrons were excited from the background electrons in the region $(r,z) = (0,25) - (35,30)\,\mu$m.

Figure 1(a) displays the initial profiles, which are spherically symmetric about $z_0 = 140$ μm. The initial plasma conditions represent an optimistic fast-ignition fuel assembly, in which no high-pressure "jet" coming from the core to the cone pushes the critical surface far from the fuel. All ions are fully ionized, which is reasonable given that we only use C and D ions and the initial temperature is >100 eV. The domain extends from $(r,z) = (0,0) - (100,240)\,\mu$m, the grid spacing was 0.5 μm except for an expansion of the r spacing to 1 μm over the first 5 μm to reduce spurious B fields near axis. The time step was 0.7 fs, and the run took 200 minutes of wall time on 38 Opteron cpu's to reach 7 ps of run time.

Figure 1(b) shows for several runs the fuel heating, or increase in background thermal energy in the "ignition region" of $(r,z) = (0,80) - (30,120)\,\mu$m. Our base case (solid black curve) has a C-D (equal parts atomic) plasma everywhere, and beam divergence $\Delta\theta = 35°$. About 30% of the beam energy gets deposited in the ignition region. The final pressure, and background T_e at several times, are shown for this run in Fig. 2. Turning off magnetic forces (solid green) on all species reduces the coupling efficiency to 13%. Replacing C-D with pure D and keeping the same mass density (and thus electron density) slightly increases the coupling to 34%. One might expect a decrease in resistive B fields with pure D due to the lower Z, and thus a reduction in magnetic collimation and finally coupling. A possible reason this does not happen is that although the average Z and resistivity are lower, the increased ion number density means the heat capacity of pure D is increased. Thus, the plasma stays cold and more resistive longer.

The CD and D cases were rerun with magnetic forces and a larger angular spread of $\Delta\theta = 60°$, giving the dashed black and red curves. They are close to each other, and the no magnetic force run. To mitigate the reduced coupling, we inserted into the pure-D case a pure-C "wire" from $(r,z) = (0,0) - (30,70)\,\mu$m, and smoothly varied the composition from C to D over 5 μm. A pinching azimuthal B is generated due to the radial resistivity gradient at the C-D interface (see Fig. 3). The resulting coupling (dashed blue curve) increases to about 21%. This shows the potential benefits of tailored material profiles to compensate for a poorly-collimated beam.

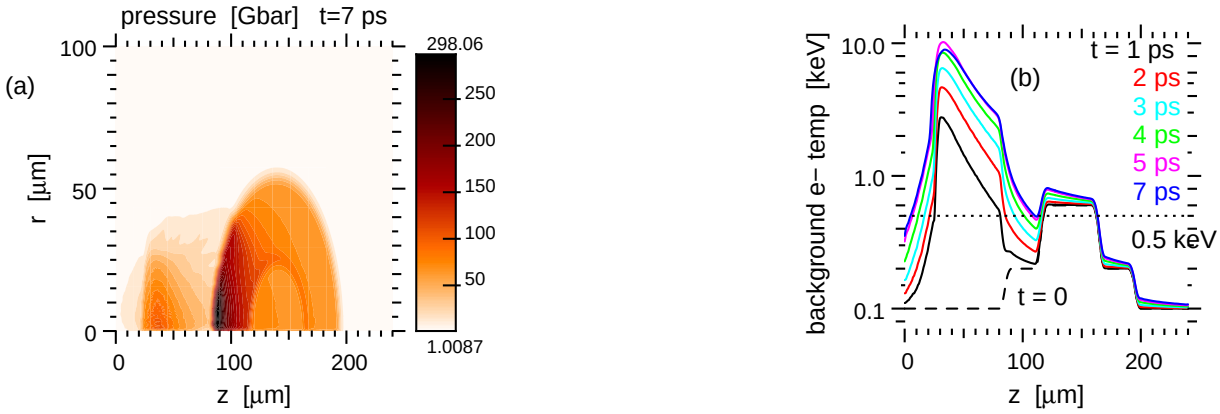

Figure 2. (a) Final (t=7 ps) background pressure profile for base case. (b) background electron temperature, averaged from $r = 0 - 10\,\mu$m, for several times for base case.

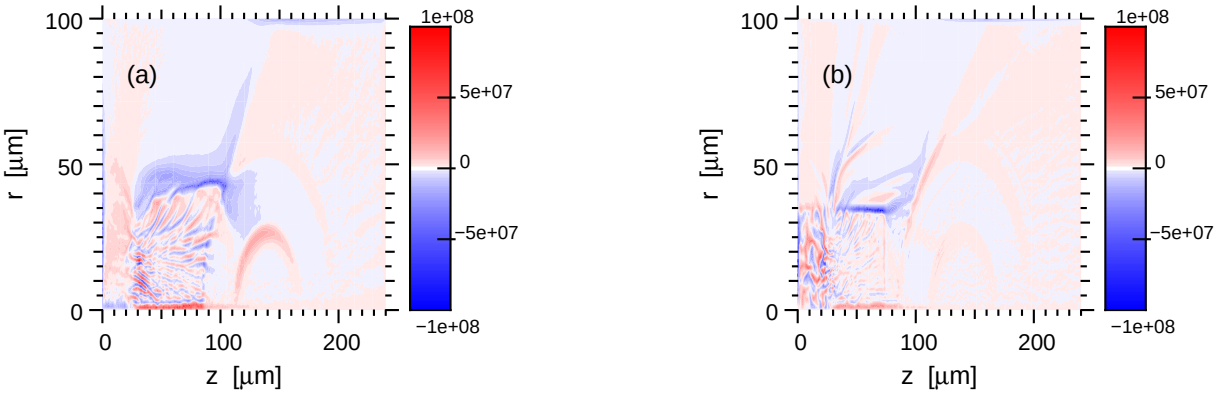

Figure 3. Azimuthal magnetic field B_θ at $t = 5$ ps for (a) base case and (b) D plasma, $\Delta\theta = 60°$, with C wire (dashed blue curve from Fig. 1(a)). $B_\theta < 0$ gives an inward radial force on electrons.

These results suggest the energy coupling for plausible electron beams and targets can be 20-30%. We are extending this work to more realistic configurations, and the full ignition problem.

Acknowledgments

We thank L. I. Divol, A. B. Langdon, and D. R. Welch for fruitful discussions. This work prepared by LLNL under Contract DE-AC52-07NA27344, LDRD tracking number 07-SI-001.

References

[1] Tabak M, Hammer J, Glinsky M E, Kruer W L, Wilks S C, Woodworth J, Campbell E M, Perry M D and Mason R J 1994 *Phys. Plasmas* **1** 1626–1634
[2] Langdon A B and Barnes D C 1985 *Multiple Time Scales* ed Brackbill J U and Cohen B I (Orlando, FL: Academic Press, Inc) pp 335–375
[3] Welch D R, Rose D V, Cuneo M E, Campbell R B and Mehlhorn T A 2006 *Phys. Plasmas* **13** 063105
[4] Hewett D W and Langdon A B 1987 *J. Comput. Phys.* **72** 121–155
[5] Cohen B I, Langdon A B and Friedman A 1982 *J. Comput. Phys.* **46** 15
[6] Manheimer W, Lampe M and Joyce G 1997 *J. Comput. Phys.* **138** 563–584 ISSN 0021-9991
[7] Lemons D S, Winske D, Daughton W and Albright B 2009 *J. Comput. Phys.* **228** 1391–1403
[8] Atzeni S, Schiavi A and Davies J R 2009 *Plasma Phys. Controlled Fusion* **51** ISSN 0741-3335
[9] Solodov A A and Betti R 2008 *Physics. Plasmas* **15** 042707